Supplementary Information (SI) for Nanoscale Advances.
This journal is © The Royal Society of Chemistry 2026

Aquaporin embedded suspended lipid bilayer on anodized alumina nanoporous substrates for studying the stability and functionality- towards the development of miniaturized water purifier

Akanksha Kumari[a], Jaydeep Bhattacharya[b], Ranjita Ghosh Moulick[a]***

[a]Amity Institute of Biotechnology, Amity University Haryana, 122413, India;

[b]School of Biotechnology, Jawaharlal Nehru University, New Delhi, 110067, India;

Supplementary Information

1.1 Florescence Recovery After Photobleaching (FRAP) on porous substrate

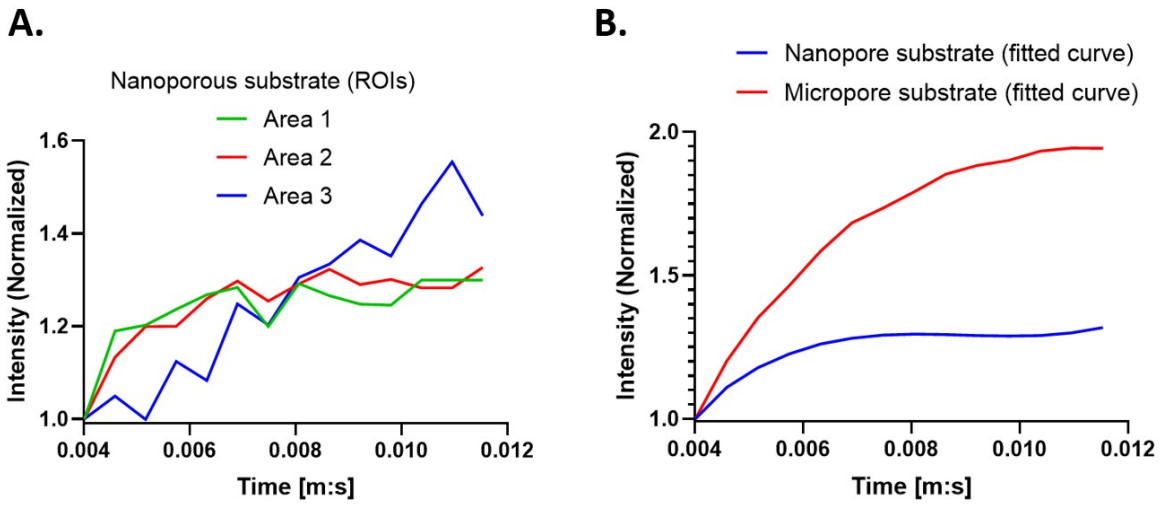

Figure S1. (A) FRAP recovery curves for nanoporous substrates showing fluorescence recovery in three ROIs: green (Area 1), red (Area 2), and blue (Area 3). (B) Comparison of fluorescence recovery on nanoporous (blue) and microporous (red) substrates.

The FRAP analysis on the nanoporous substrate shows the limitations due to its nanoscale resolution. The inherent difficulty was defining precise regions of interest (ROIs) for photobleaching under the confocal microscope, which operates at a microscale resolution, led to irregular recovery patterns. The zigzag nature of the fluorescence recovery curves across the three ROIs (Area 1, Area 2, Area 3) can be observed in Figure S1(A). Despite the irregularities, the fitted curves to these recovery patterns revealed an overall increase in fluorescence intensity over time, confirming the lateral mobility of lipid molecules labelled with DHPE Texas Red within the bilayer. This result underscores the presence of dynamic lipid behaviour on the nanoporous substrate, albeit with reduced precision in results. In contrast, the FRAP

experiment on the microporous substrate was easier, as the microscale dimensions of the pores aligned well with the resolution of the confocal microscope. This compatibility allowed for accurate photobleaching and monitoring of fluorescence recovery in a well-defined ROI. The resulting recovery curve displayed a smooth, gradual increase in fluorescence intensity over time, enabling a precise determination of recovery kinetics (Figure S1(B)). When comparing the nanoporous and microporous substrates, the microporous system exhibited more uniform fluorescence recovery. The curve fit indicate intensity recovery better than on nanoporous substrate.

During the FRAP experiment, the bilayer is labelled with fluorescent molecules (e.g., Texas Red), and a high-intensity laser is used to photobleach a defined Region of Interest (ROI). The fluorescence intensity is then measured as it recovers over time. The recovery curve is used to extract several important parameters, including the half-time ($\tau_{1/2}$), mobile fraction (MF), immobile fraction (IF), and ultimately, the diffusion coefficient (D).

Solid Glass Substrate: On solid substrates, the bilayer is stable, with clear and consistent fluorescence recovery. The recovery curve follows a well-defined pattern that can be easily analysed using the standard equations. The diffusion coefficient (D) for lipid mobility in solid substrates is typically extracted using the formula:

$$D = \frac{w^2 * 0.88}{4 * \tau_1/_2}$$

For solid glass, the diffusion coefficient is approximately 1.6-1.8 $\mu m^2/s$, which is in line with previous studies on solid lipid bilayers [1-3].

Microporous Substrate: The microporous substrate with the larger pore sizes can result in partial bilayer formation and fragility. As a result, the recovery curves may show comparable recovery but with some irregularities, with a measured value of approximately 1.7 $\mu m^2/s$ in this study.

Nanoporous Substrate: The recovery curve on nanoporous substrates is more complicated. The small pore sizes (nanoscale) lead to irregular fluorescence recovery patterns due to the limited resolution of confocal microscopy. This makes defining the Region of Interest (ROI) challenging, especially when trying to observe recovery in such small pores. As shown in Figure S1(A), the recovery curves exhibit a zigzag pattern across different regions, which makes it difficult to extract precise parameters. The difficulty in defining ROIs on nanoporous substrates results in irregular recovery curves, making it challenging to accurately extract half-time in this case.

1.2 Pore Coverage Under Different Experimental Conditions

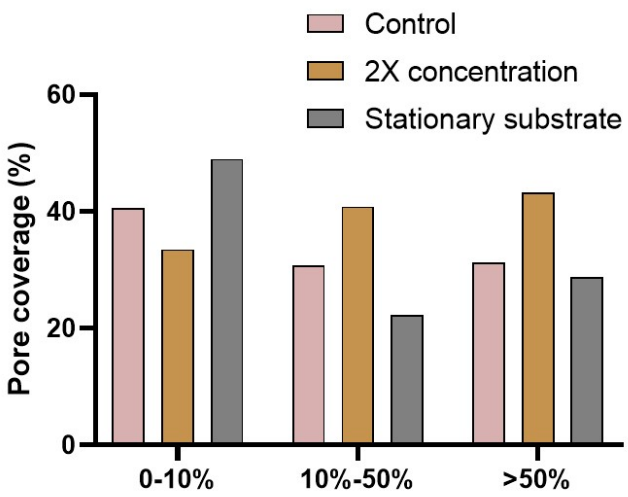

Figure S2. Percentage of pore coverage categorized into 0%-10%, 10%-50%, and >50% under three experimental conditions: Control (pink), 2X Concentration (orange), and Stationary substrate (grey).

The bar chart illustrates the percentage of pore coverage under three experimental conditions: Control, "2X Concentration", and "Stationary substrate" conditions. The control represents the experimental setup with no approach, while 2X Concentration and Stationary substrate are strategies implemented to improve pore coverage and bilayer stability. In the 2X Concentration approach, increasing the lipid concentration improved initial pore coverage, with 58.73% of pores showing >50% coverage on Day 0 (D0), higher than the Control (55.50%). However, by Day 1 (D1), bilayer stability decreased significantly, with >50% coverage dropping to just 3.62%, and 72.56% of pores showing minimal coverage (0%-10%). These results indicate that while higher lipid concentration enhances initial coverage, it does not address the temporal instability of the bilayer, as seen in the Control condition where >50% coverage fell from 55.50% on D0 to only 2% on D1. In comparison, the Stationary substrate approach, where the system was left overnight without disturbances, demonstrated the highest improvement in bilayer stability. On D0, 64.12% of pores had >50% coverage, which decreased more gradually to 22.32% by D1. This approach also had the lowest proportion of pores with minimal coverage (0%-10%) on D1, at 59.65%. These results show that the undisturbed base condition provided some improvement in stability among the tested methods. Overall, while both approaches improved initial pore coverage compared to the Control.

1.3 Homogeneous Distribution of Aquaporin in Model Membranes

In our model membrane system, aquaporin—a native transmembrane protein—exhibits a homogeneous distribution, as confirmed by via fluorescence microscopy tagged with Alexa Fluor 488 (Fig. 8A). This contrasts with previous observations involving hemoglobin, a non-membranous protein, exhibit heterogeneity and tend to form supramolecular aggregates within similar POPC lipid environments [4]. The distinct behaviour is attributed primarily to the

inherent polarity nature of membrane proteins such as aquaporins, which integrate seamlessly into the lipid bilayer. Their transmembrane domains anchor within the hydrophobic core of the membrane, minimizing clustering and promotes uniform distribution in lipid environment (Fig. S3).

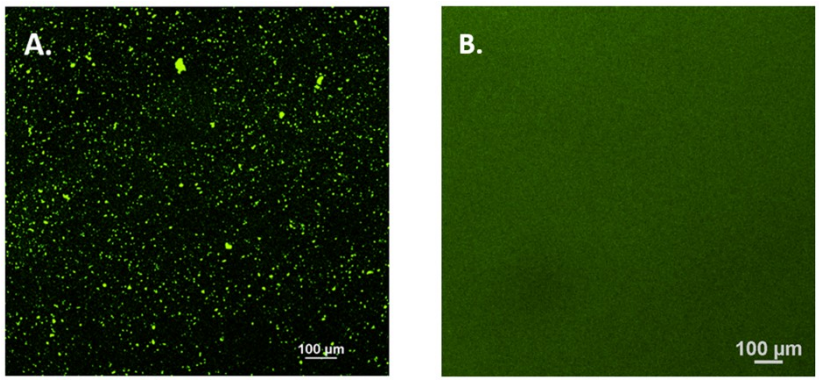

Figure S3. Distribution of Alexa Fluor 488-labeled proteins in POPC lipid bilayers (A) Hemoglobin (B) Aquaporin (AQP)

1.4 Determination of Diffusion Coefficient (D) and Related Parameters

In the initial (pre-bleach) phase, a defined region of interest (ROI) within the bilayer containing Texas Red fluorescent molecules was illuminated with a low-intensity laser to record the initial fluorescence intensity (F_i). A brief, high-intensity laser pulse was then applied to irreversibly photobleach the fluorophores in this region, reducing the signal to a lower value (F_0). The resulting intensity data were processed using min–max normalization to facilitate comparison across experiments.

$$Normalized\ Value\ = \frac{Original\ Value - \ Min\ Value}{Max\ Value - Min\ value} \quad \text{...Eq. (S1)}$$

Fluorescence recovery within the ROI, driven by the lateral diffusion of unbleached molecules from surrounding areas, was recorded over time and fitted to a stretched exponential model:

$$Y_{fit} = A\left(1 - \exp\left(-k * t^{n}\right)\right) \quad \text{...Eq. (S2)}$$

Here, A is the maximum recovery amplitude, k is the rate constant, t is time, and n is a stretching exponent capturing deviations from simple exponential kinetics. Recovery proceeded until a stable plateau (F_∞) was reached.

From the recovery curve, several parameters were derived:

Half-time of recovery ($\tau_{1/2}$), time to reach half of the maximal recovery ($F_{1/2}$).

$$F_1/_2 = \frac{F_0 + F_\infty}{2} \quad \text{…Eq. (S3)}$$

Mobile fraction (MF), fraction of fluorophores capable of diffusing into the bleached ROI.

$$MF = \frac{F_\infty - F_0}{F_i - F_0} \quad \text{…Eq. (S4)}$$

Immobile fraction (IF), fraction that remains non-mobile.

$$IF = 1 - MF \quad \text{…Eq. (S5)}$$

Finally, the diffusion coefficient (D) was calculated from $\tau_{1/2}$ using the beam radius *w* [3, 5-7].

$$D = \frac{w^2 * 0.88}{4 * \tau_1/_2} \quad \text{…Eq. (S6)}$$

Reference:

1. Afanasenkau D. Supported lipid bilayer as a biomimetic platform for neuronal cell culture [dissertation]. Forschungszentrum Jülich; 2013.
2. Kang M, Day CA, Kenworthy AK, DiBenedetto E. Simplified equation to extract diffusion coefficients from confocal FRAP data. Traffic. 2012;13(12):1589–1600.
3. Kumari A, Kumar S, Aswal VK, Bhattacharya J, Sen S, Ghosh Moulick R. Protein–lipid interactions in a three-component POPC–cholesterol–sphingomyelin modulated membrane. J Phys Chem B. 2025;129(40):10298–10310.
4. Kumari A, Saha D, Bhattacharya J, Aswal VK, Moulick RG. Studying the structural organization of non-membranous protein hemoglobin in a lipid environment after reconstitution. Int J Biol Macromol. 2023; 243:125212.
5. Kang M, Day CA, Kenworthy AK, DiBenedetto E. Simplified equation to extract diffusion coefficients from confocal FRAP data. Traffic. 2012;13(12):1589–1600.
6. Axelrod D, Koppel DE, Schlessinger J, Elson E, Webb WW. Mobility measurement by analysis of fluorescence photobleaching recovery kinetics. Biophys J. 1976;16(9):1055–1069.
7. Lorén N, Hagman J, Jonasson JK, Deschout H, Bernin D, Cella-Zanacchi F, Braeckmans K. Fluorescence recovery after photobleaching in material and life sciences: putting theory into practice. Q Rev Biophys. 2015;48(3):323–387.